Materials and Design 114 (2017) 416–423

Contents lists available at ScienceDirect

Materials and Design

journal homepage: www.elsevier.com/locate/matdes

Tuning crystalline structure of zeolitic metal–organic frameworks by supersonic spraying of precursor nanoparticle suspensions

Bhavana N. Joshi [a,1], Jong-Gun Lee [a,1], Seongpil An [a], Do-Yeon Kim [a], Ji Sun Lee [b], Young Kyu Hwang [b], Jong-San Chang [b,c], Salem S. Al-Deyab [d], Jin-Chong Tan [e,*], Sam S. Yoon [a,*]

[a] School of Mechanical Engineering, Korea University, Seoul 136-713, Republic of Korea
[b] Res. Group for Nanocatalysts, Korea Res. Inst. of Chem. Tech., Daejeon 305-600, Republic of Korea
[c] Dept. of Chem., Sungkyunkwan University, Suwon 440-476, Republic of Korea
[d] Petrochem. Research Chair, Dept. of Chem., King Saud Univ., Riyadh 11451, Saudi Arabia
[e] Multifunctional Materials & Composites (MMC) Laboratory, Dept. of Engineering Science, University of Oxford, Parks Road, Oxford OX1 3PJ, United Kingdom

HIGHLIGHTS

- Zeolitic Imidazolate Framework-7 (ZIF7) films have been fabricated by a supersonic cold-spraying method.
- Crystalline structures of the supersonically sprayed ZIF7 film can be controlled by adjusting the nylon content.
- Supersonic spraying technique is versatile, it can be used to fabricate ZIF7 phase-I, -II, and -III.
- Inclusion of 6 wt% of nylon improves framework mechanical stability, preventing phase changes upon high-energy impact.

GRAPHICAL ABSTRACT

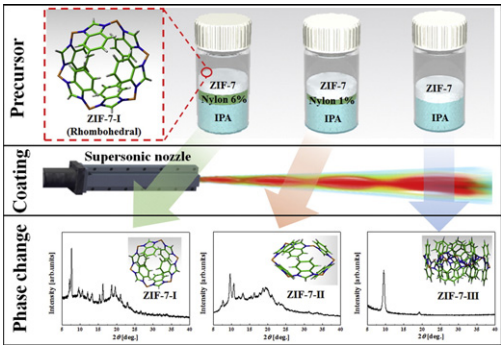

ARTICLE INFO

Article history:
Received 8 July 2016
Received in revised form 28 October 2016
Accepted 1 November 2016
Available online 6 November 2016

Keywords:
Supersonic spraying
Metal organic framework
Phase transformation
Zeolitic imidazolate framework
Mechanical properties

ABSTRACT

The deposition of sodalite zeolitic imidazolate framework-7 (ZIF7) films by a supersonic cold-spraying technique was successfully accomplished for the first time. The high-speed impact of supersonic cold spraying increased the monodispersity of the ZIF7 crystalline structure. However, the intensity of the structural change decreased with increasing the amount of nylon in the ZIF7 suspension. Mitigating phase changes in ZIF7 occurred by the impact dampening conferred by the polymeric nature of nylon, which preserved the original three-dimensional crystalline structure of ZIF7. The inclusion of *N*,*N*-dimethylformamide (DMF) in a nylon–ZIF7 suspension improved the dispersion of ZIF7 nanoparticles, which in turn eliminated the dampening effect from the nylon and recovered the distinctive monodispersity arising from the high-speed impact. This characteristic was observed at all impact speeds for ZIF7 suspensions containing DMF. We show that high-rate cold spraying of ZIF7 particles can be combined with nylon and other pressure-transmitting media to control the formation of three distinctive phases. The unique capability to tune the crystalline structure of ZIF7 allows customization of the film functionality for specific applications.

* Corresponding authors.
E-mail addresses: jin-chong.tan@eng.ox.ac.uk (J.-C. Tan), skyoon@korea.ac.kr (S.S. Yoon).
[1] These authors have contributed equally.

http://dx.doi.org/10.1016/j.matdes.2016.11.001
0264-1275/

1. Introduction

Zeolitic imidazolate frameworks (ZIFs) are three-dimensional (3D) assemblies of metal ions and imidazole-based organic ligands, whose porous open frameworks mimic those of (inorganic) aluminosilicate zeolites. The crystal structure of ZIFs is analogous to that of zeolites because of the bond-angle resemblance between metal–linker–metal bonds and Si–O–Si linkages, both of which subtend angles of 145° [1]. The combination of metal and organic linkers in ZIFs yields porous materials with high surface areas and tunable functionalities, along with a good combination of thermal and chemical stability [2]. Thus, they can potentially be used in different practical applications such as sensors, catalysts, adsorbents, matrix fillers, membranes, and drug delivery [3–5].

Zinc 2-benzimidazolate (ZIF7) is formed by linking benzimidazolate (bIm) anions to divalent Zn^{2+} cations. First discovered by Huang et al. [6], ZIF7 has a sodalite topology with hexagonal symmetry [7]. It is distinct from Zinc 2-methylimidazole (ZIF8), which also adopts a sodalite topology, because of the presence of a phenyl group in the bIm ligand of ZIF7 [8,9]. The pore window size of ZIF7 is 0.30–0.35 nm, thus allowing access of CO_2 molecules over N_2 and showing high selectivity for CO_2 [10]. ZIF7 is capable of CO_2 separation from NO_2 [10] at relatively low pressures and temperatures and from alkanes/alkenes through a gate-opening process [11]. ZIFs display structural flexibility because of their weaker coordination bonds. The mechanical properties of ZIFs (Young's modulus, hardness, and bulk modulus) [12] are approximately one order of magnitude lower than those of inorganic zeolites [13]. Because of the flexibility of the framework, ZIFs can undergo structural transformations or phase changes under high pressures or temperatures, as well as after the adsorption of gas molecules. Aguado et al. [14] and Zhao et al. [15] described the large- to narrow-pore transformation of ZIF7 by gas adsorption induced by temperature and pressure, respectively. Wharmby et al. [16] recently reported the porous-to-dense phase transition of desolvated ZIF4. The phase transition in ZIF4 is due to the rotation of imidazolate linkers, which causes volumetric contraction of pores. The collective lattice dynamics (THz vibrations) and soft modes present in ZIF7 can also cause gate-opening phenomena and trigger mechanical instability, causing shear-induced structural collapse and framework amorphization [17].

The crystal morphology of metal–organic frameworks (MOFs) can be controlled by selecting particular synthesis conditions or processing routes. For example, Low et al. [18] demonstrated that a crystal–to–crystal phase transformation occurred when ZIF-L crystals were transformed to ZIF8 crystals under different solvents and heating processes. This transformation is called a topotactic phase transition, in which a crystalline material undergoes structural changes but the final phase is related to the initial crystal structure by similar crystallography or orientation.

Synthesizing ZIF7 as films or membranes on porous Al_2O_3 or polymer-based membranes [19] makes such films attractive for sensing, adsorption, and gas separation applications [3,20,21]. For the fabrication of ZIF membranes and films, the main approaches used are direct synthesis and secondary growth methods. However, very few methods have been reported for the deposition of ZIF7 films [22]. Melgar et al. [1] deposited ZIF7 films by an electrospraying technique on an Al_2O_3 substrate and observed the formation of ZnO when the substrate temperature was maintained at 160 °C. Peng et al. [23] reported the fabrication of ZIF7 molecular sieve nanosheets that were exfoliated by wet ball milling; the membranes were then deposited on porous α-Al_2O_3 substrates. The prepared membranes were subsequently used for H_2 gas permeance and selectivity. However, these methods are not easily scalable for use in commercial production and industry.

Herein, we report for the first time the use of cold spraying, a fast and highly scalable method, for the deposition of ZIF7 films [24,25]. In the cold-spraying technique, particles are injected into a supersonic gas stream and accelerated to supersonic velocities [26,27]. These high-velocity particles collide with the substrate with substantial kinetic impact energy, resulting in strong adhesion of the particles to the substrate. This is a high-rate coating method with apparatus details discussed in an earlier report [28]. The goal of this investigation was to study the influence of cold-spray impact pressure and the effects of different solvents on the structural properties of ZIF7. We have discovered distinctive changes in the crystalline structure upon supersonic impact of ZIF7 particles, with and without the application of nylon and *N*,*N*–dimethylformamide (DMF) in the suspension precursor.

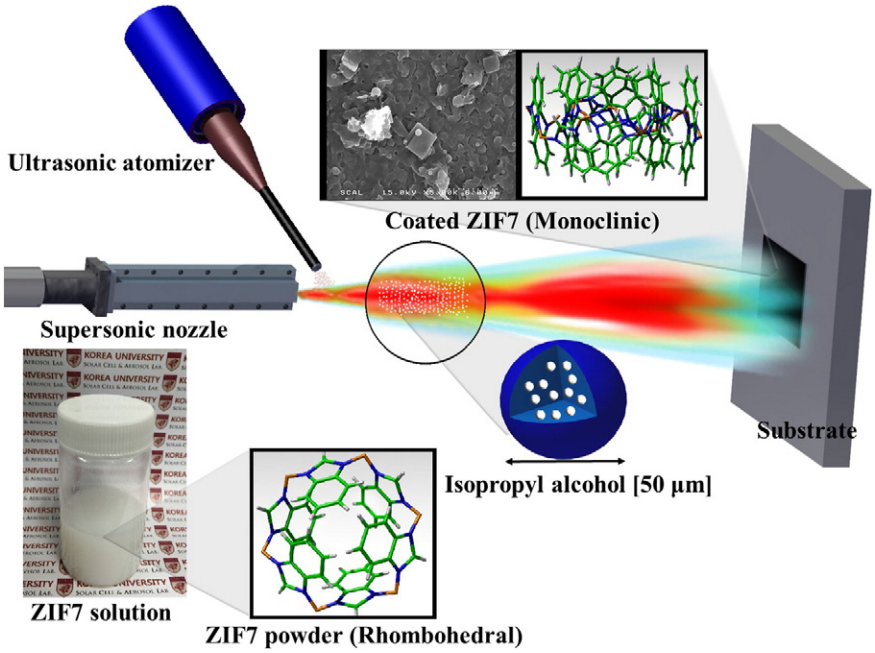

Fig. 1. Graphical illustration of the supersonic cold-spraying ZIF7 process.

2. Experimental methodology

2.1. Precursor suspensions

ZIF7 nanoparticles were suspended in various solvents and sprayed onto a copper substrate via supersonic cold spraying. Three different sets of colloidal solutions were prepared, each using 1 g of ZIF7 powder. The first suspension was ZIF7 in 50 mL of isopropyl alcohol (IPA), denoted as I–ZIF7. In the second suspension, various concentrations (1 and 6 wt%) of nylon–6 were added to the I–ZIF7 solution, denoted as N–ZIF7. To improve the dispersion of the ZIF7 nanoparticles, 10 mL of DMF was added to the N–ZIF7 solution, denoted as D–ZIF7. These three types of suspensions were sonicated (Pronextech, South Korea) for 2 min to achieve homogeneous dispersions of ZIF7 nanoparticles in the solutions prior to cold spraying.

2.2. Supersonic cold spraying

The ZIF7 films were deposited by means of a supersonic spray-coating system (also known as the cold-spray method), as shown in the schematic in Fig. 1, by using ZIF7 powder (particle sizes of 100–150 nm). A typical cold-spray system consists of a gas tank, gas heater, supersonic nozzle, ultrasonic atomizer, syringe pump, and X–Y translation stage [29].

The prepared precursor was pumped by a syringe pump (KDS LEGATO 210, Sercrim Lab. Tech. South Korea) toward the nozzle via an ultrasonic liquid processor (VCS134ATFT, Sonic & Materials, Inc., USA). The feed solution (sol) was discharged in an undifferentiated, supersonic air stream through the nozzle, which accelerated the sol toward the substrate; a uniform coating was generated by means of four cycles of deposition with a substrate area coverage of 15 cm^2/min. The operating air pressure (P_0) was varied from 2 to 7 bar (200 to 700 kPa) and the heater temperature (T_0) for the air was varied from 150 to 450 °C. The ZIF7 nanoparticles gained high kinetic energy from the hot compressed air blown through the supersonic nozzle, which yielded well-adhered, compact ZIF7 films on the substrates. The ZIF7 films were coated onto copper substrates with an average thickness of ca. 20 μm.

2.3. Materials characterization

The structural phase transformations of ZIF7 were studied using an X–ray diffractometer (Rigaku, SmartLab) using Cu Kα radiation for $2\theta = 5°$ to 40°. The surface morphology and surface roughness of the deposited films were determined using a high-resolution scanning electron microscope (HR–SEM, S–5000, Hitachi Co., Japan) at 15 kV and an atomic force microscope (AFM, XE–100, Park Systems, Korea), respectively. Raman spectroscopy was performed using a confocal Raman spectrometer (NRS-3100) with a laser source of 532 nm. The thermal stability of the films was measured using a thermogravimetric analyzer (TGA, Q–500, TA Instruments, USA). For TGA, the sample of ~2–3 mg in mass was held in a platinum pan under N_2 atmosphere using a heating rate of 10 °C/min.

3. Results and discussion

The crystal structures of the cold-sprayed ZIF7 powder and ZIF7 films with varying concentrations of nylon (0, 1, and 6 wt%) are identified by X-ray diffraction (XRD), as shown in Fig. 2. The XRD pattern of the pristine as-synthesized ZIF7 powder exhibits characteristic peaks at 2θ = 7.15, 7.65, 10.31, 12.09, 13.03, 15.37, 16.25, 18.64, 19.60, 21.10, 23, and 26°, corresponding to the specific Miller indices shown in Fig. 2, which confirm that the powder is ZIF7 Phase I [11,15,30,31]. The nylon used in the solvent and films was deposited at $P_0 = 2$ bar (200 kPa) and $T_0 = 250$ °C. Without the nylon content, the IPA solvent is expected to evaporate because of the high temperature and pressure; the high-speed impact of ZIF7 on the substrate thus transforms the powder to a different phase. This phase shows an intense peak at $2\theta = 9.6°$, which matches the ZIF7 Phase III reported by Zhao et al. [15]. ZIF7 Phase III features a two-dimensional (2D) layered architecture, which is significantly denser and more stable [32] compared with the porous structure of Phase I. Peng et al. [23] applied ball milling to ZIF7 nanoparticles and suggested that the 3D phase III was transformed to a 2D structure by the breaking of coordination bonds in the six-membered rings of ZIF7, thereby leaving a framework containing only four-membered rings. They described this resultant phase as the 2D stacking of ZIF7 layers along the (002)-oriented c-axis. Indeed, this delamination process occurred because of the lower-energy impact deformation caused by the wet ball milling of ZIF7, performed for nanosheet exfoliation. In the current study, it is proposed that the high-velocity mechanical impact facilitates the aforementioned 3D-to-2D framework conversion. We reasoned that a combination of shear and compressive stresses arising from the high-velocity impact causes the formation of ZIF7 Phase III, as evidenced by the strongly textured film with (002) facets corresponding to the very distinct 2θ peak at 9.6° (Fig. 2).

When the nylon concentration in the precursor suspension is 1 wt%, the phase changes from polycrystalline ZIF7 (Phase I) to mixed-phase ZIF7 (Phase II), which shows peaks at $2\theta = 9.6$ and 10.31°, along with other peaks matching those of Phase I in ZIF7, which resemble those of the pure powder. These mixed-phase peaks of ZIF7 are consistent with the peaks of ZIF7 Phase II reported by Zhao et al. [15], who applied thermal heating at 427 °C to yield the phase change. When the concentration of nylon is increased to 6 wt%, phase I is preserved, as confirmed by the Bragg peak at 7.5°. These results may arise from the nylon acting

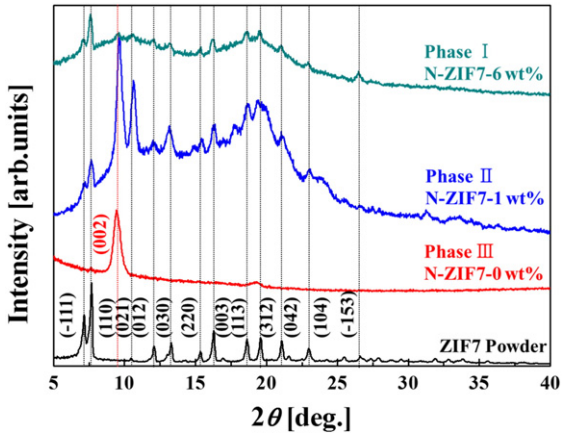

Fig. 2. XRD patterns showing the effect of nylon concentration from 0 to 6 wt% on film crystal structures.

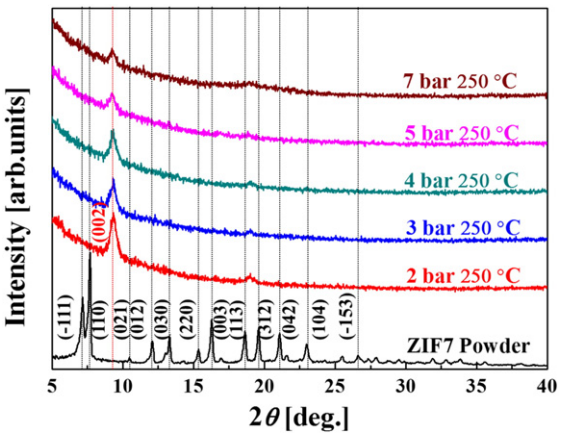

Fig. 3. XRD patterns of the film crystal structures of the I–ZIF7 precursor (without nylon) at supersonic cold-spray pressures of 2–7 bar (200–700 kPa).

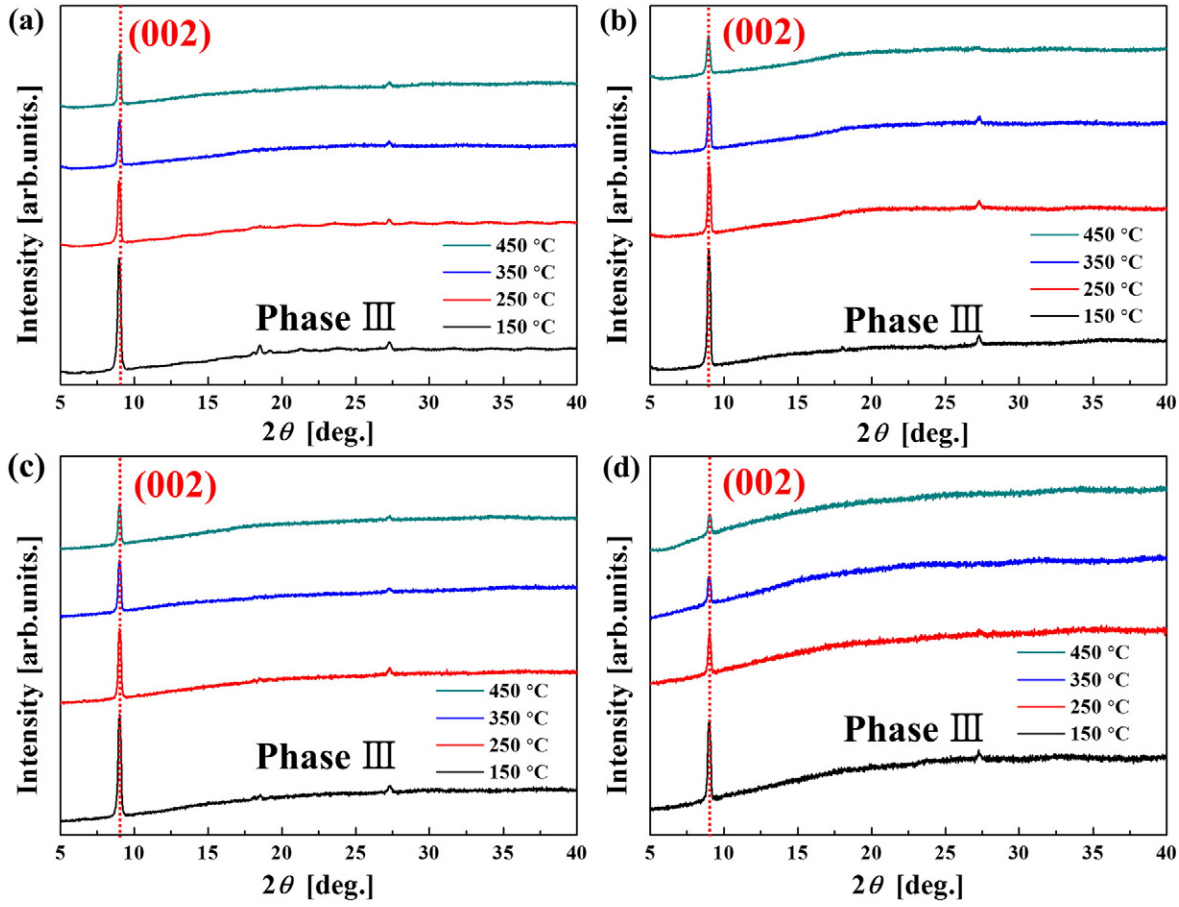

Fig. 4. XRD patterns of film crystal structures of D–ZIF7 with 6 wt% nylon at varying operating temperatures and pressures of (a) 2, (b) 3, (c) 4, and (d) 5 bar (200, 300, 400, and 500 kPa).

as an intermolecular binder that lowers the impact pressure of ZIF7 by forming a protective sac, thereby improving the overall mechanical stability of the nanoparticles, as explained in the next section. When the nylon concentration is low, the ZIF7 particles collide with the substrate at partial pressure; however, nylon still somewhat lowers the effect of impact during particle-to-substrate collision, and thus the product obtained appears to be mixed-phase ZIF7.

When dispersed in IPA without nylon, the ZIF7 particles undergo structural transformations directly to Phase III, as shown in Fig. 3, showing the importance of the impact pressure generated by supersonic cold spraying. The intensity of the peak appearing at 9.6° at $P_0 = 2$ bar (200 kPa) systematically decreases with increasing pressure because of the gradual loss of long-range order (crystallinity) in the ZIF7 structure. The poor crystallinity of ZIF7 is caused by the collapse of the

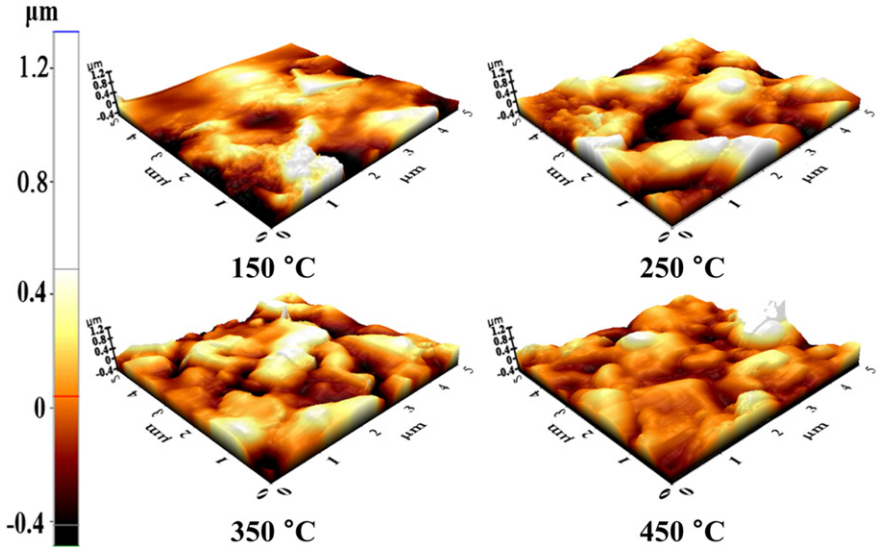

Fig. 5. Surface roughness from AFM images of the cold-sprayed films at various impact speeds controlled by the operating gas temperature (150 °C ≤ T_0 ≤ 450 °C). The gas pressure was fixed at $P_0 = 2$ bar (200 kPa).

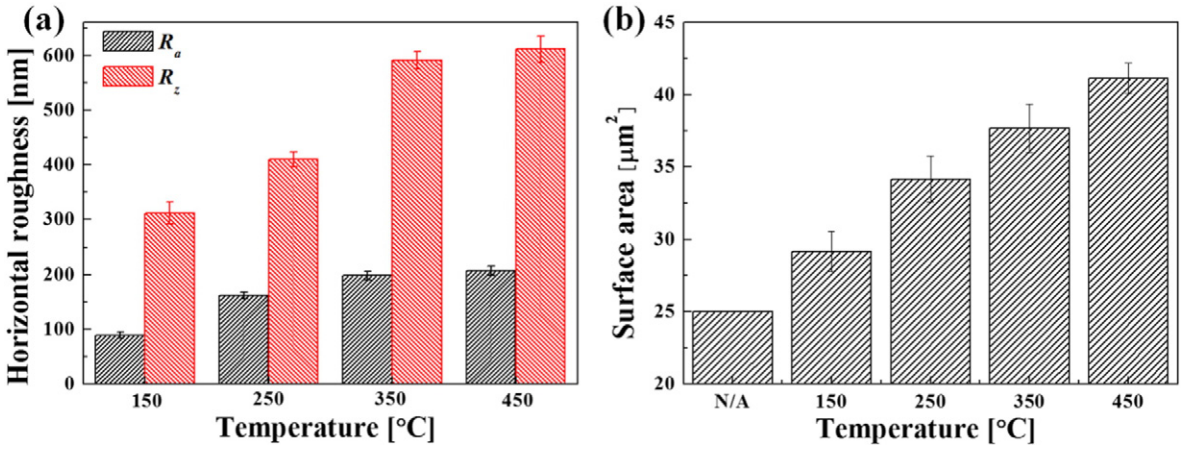

Fig. 6. (a) Surface roughness and (b) area of ZIF7 films for 150 °C ≤ T_0 ≤ 450 °C. The gas pressure is fixed at P_0 = 2 bar (200 kPa).

framework from collisions of ZIF7 particles with the substrate at very high impact velocities and elevated strain rates, which we suggest is the result of the thermo-mechanical deformation that causes the structural collapse responsible for amorphization [33,34]. The particles injected into the supersonic air stream coming through the *de Laval* convergent–divergent nozzle attain velocities ranging from 300 to 500 m/s depending on the pressure and temperature [35]. Such high impact pressures facilitate the adhesion of particles on the substrate, but they also induce fracture in the particles, as mentioned in our previous study [24].

We established that the use of DMF in the colloidal solution improved the dispersion of the ZIF7 nanoparticles. The XRD patterns presented in Fig. 4 clearly reveal that including DMF in the N–ZIF7 suspension minimizes the effect of nylon, thus suppressing the recovery of the original XRD peaks of the pure ZIF7 powder. Phase III [15,23] is confirmed by the dominant peak appearing at $2\theta = 9.6°$. Thus, it is clear that DMF directly acts as a pressure-transmitting fluid. No significant effect of IPA, nylon, or both is observed on the phase transformation, and thus the effect of high-speed pulverization of the supersonic spray is dominant in causing the phase transformation. As compared to I–ZIF7 in Fig. 3, the inclusion of nylon and DMF in the precursor suspension also reduces the amorphization rate of ZIF7, both of which thus improve the mechanical stability of the ZIF7 nanoparticle by enhancing its structural resistance to pore collapse under impact stress.

Notably, the formation of ZnO indicates an increase in density. ZnO formation is often induced when carbon degrades at high processing temperatures, in which case the porous MOF structure begins to collapse, forming a dense structure. Although supersonic cold spraying is performed at high gas temperatures, all thermal energy is converted into kinetic energy, and thus the static temperature near the substrate is higher than room temperature. This low processing temperature (thus the name supersonic "cold" spraying) prevents the formation of ZnO.

The 3D AFM morphologies of D–ZIF7 films deposited at P_0 = 2 bar (200 kPa) at different temperatures are presented in Fig. 5. The peaks and valleys in the AFM images are ascribed to random lateral ZIF7 stacking. The films clearly show increasing surface roughness with decreasing particle size, which is varied with variations in the high impact energy of the supersonic cold spraying. The arithmetical mean roughness values (R_a) determined from the AFM images are shown in Fig. 6(a). The roughness is increased with increasing air temperature, whereas the ten-point median roughness (R_z) values are observed to vary significantly. Fig. 6(b) shows the surface areas of the uncoated copper substrate and the films deposited at increasing temperatures and a constant pressure of P_0 = 2 bar (200 kPa), as measured using AFM [28]. The surface area increases with increasing T_0, which also increases the impact velocity and pressure by converting the increased thermal energy into increased kinetic energy. As a result, particle pulverization increases with increasing T_0.

Fig. 7 shows the SEM images of I–ZIF7 and N–ZIF7. For the I–ZIF7 film, the surface morphology shows small ZIF7 particles, with some flat surfaces created by the high impact pressure of the cold spraying. In the N–ZIF7 film, the surface morphology shows agglomerates comprising polycrystalline ZIF7 particles, as shown in Fig. 2. This is because nylon acts as an intermolecular binder that mechanically stabilizes the 3D structure of Phase I ZIF7. The polymeric nylon provides a cushioning effect that reduces the intensity of the pulverization process, as evident in Fig. 7(b). The inset in Fig. 7(b) shows the cross-sectional view of the uniform film.

Fig. 8 shows SEM images of cold-sprayed D–ZIF7 films on a copper substrate at P_0 = 2–5 bar (200–500 kPa) and different temperatures. Cubic-shaped ZIF7 particles are clearly observed up to P_0 = 3 bar

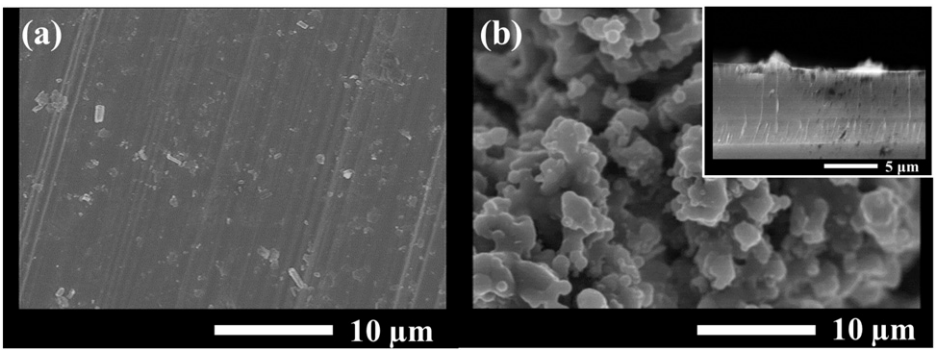

Fig. 7. SEM images of (a) I–ZIF7 and (b) N–ZIF7 films at a nylon concentration of 6 wt%, The inset shows the cross-sectional view of the film. The operating temperature and pressure are T_0 = 250 °C and P_0 = 2 bar (200 kPa), respectively. DMF is not included in the precursor suspensions.

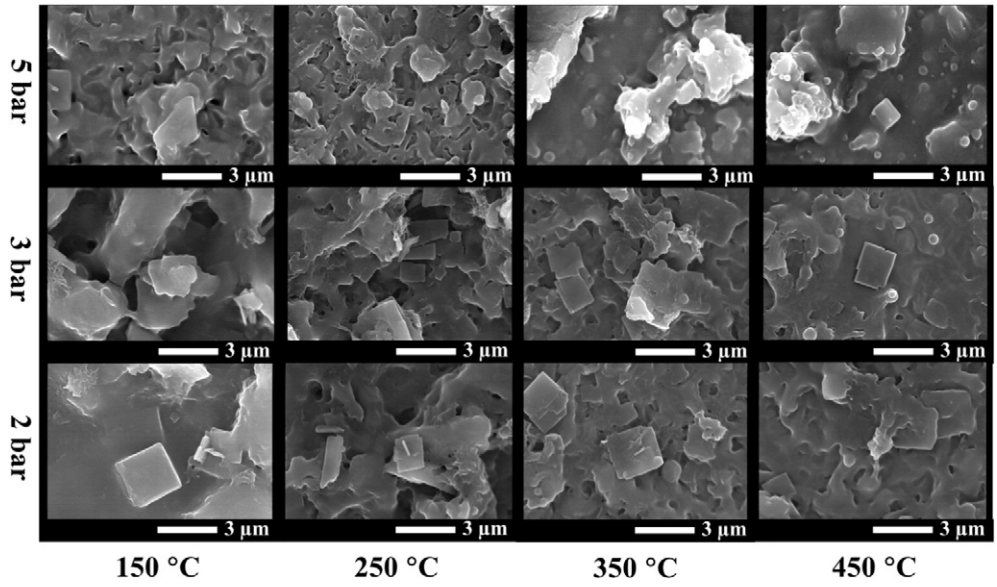

Fig. 8. SEM images showing the effect of impact speed on the surface morphology of D–ZIF7 films. The gas temperature and pressure varied in the range of 150 °C ≤ T_0 ≤ 450 °C and 2 bar (200 kPa) ≤ P_0 ≤ 5 bar (500 kPa), respectively.

(300 kPa). A thin layer of nylon and DMF covering the ZIF7 grains, forming a stiff material, is observed in all SEM images. This stiff material is melted, fractured, or both by the high impact energy of the particles. However, the grains of ZIF7 observed in the SEM images of films deposited at high air pressures and temperatures are fractured and flattened by the impact pressure. The images clearly show the change in surface microstructure with increasing gas pressure. Less porous and more agglomerated surface microstructures are observed at an air pressure of 5 bar (500 kPa). Comparing the SEM image of D–ZIF7 at $T_0 = 250$ °C and $P_0 = 2$ bar (200 kPa) in Fig. 8 with the N–ZIF7 image in Fig. 7(b), the effect of DMF inclusion is clear. The particle impact speed in the two cases is equal, because both films are acquired at the same operating temperature and pressure. As mentioned earlier, the surface morphology is much rougher when using N–ZIF7 because of the "cushioning" effect of nylon. When DMF is used, because of the improved dispersion of the particles in the precursor suspension, the pulverization process upon particle impact is much more efficient, resulting in a uniform surface morphology.

The Raman spectra of the ZIF7 films deposited from different solution configurations are presented in Fig. 9. The peaks correspond to different vibrations of the Zn–N lattice, benzene, and the imidazole ring. A comparison of the ZIF7 Raman data with the results reported by Zhao et al. [15] shows that the peaks are in good agreement. Table 1 presents the Raman frequencies and their respective band assignments. However, after spray deposition, the intensity of the Zn—N bond peak weakens, which may be the result of mechanical straining of the compliant ZnN_4 tetrahedral coordination environment prevalent in ZIF structures [36,37]. Fig. 9 shows that all Raman bands remain similar and at constant frequencies, indicating that the chemical structure of ZIF7 is unaffected.

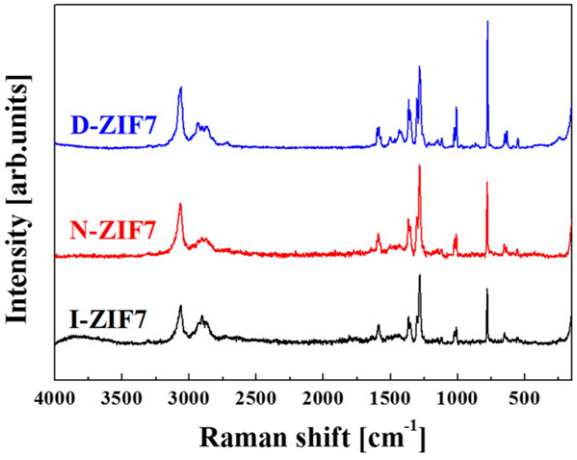

Fig. 9. Raman spectra of ZIF7 films with nylon and DMF. The pressure and temperature are fixed at $P_0 = 2$ bar (200 kPa) and $T_0 = 250$ °C, respectively.

The TGA data shown in Fig. 10 indirectly indicates the role of DMF in the collapse and retention of the crystal structure. Note that the D–ZIF7 film does not include nylon, in order to elucidate the effect of DMF alone. The thermal stability testing of the pure ZIF7 powder and the D–ZIF7 film by TGA is performed under N_2 gas at a heating rate of 10 °C/min. Fig. 10 shows three gradual steps in the weight loss of the D–ZIF7 film at 25 °C and 800 °C. Approximately 5% weight loss is observed between 25 °C and 300 °C by the removal of moisture and trapped alcohol. A weight loss of 35% is observed between 300 °C and 630 °C from the removal of DMF. The weight loss observed between 630 °C and 800 °C indicates the thermal decomposition of the structural framework of ZIF7, associated with the decomposition of the organic linkers. For the pure ZIF7 powder, 70% residue remains. However, for the D–ZIF7 film, the remaining residue is 42%. This difference in retained residue is because of the structural change of the film caused by the high-speed impact.

Table 1
Raman frequency and band assignment.

Frequency [cm^{-1}]	Band assignment
140	Zn–N
551	Stretching of benzene & imidazole ring
554	Stretching of benzene & imidazole ring
650	Torsion of imidazole ring
773	Bending of benzene & imidazole ring
1007	Bending of benzene ring
1268	Bending of benzene & imidazole C—H
1351	Stretching of C—N
1573	Bending of N—H
2900–3050	Stretching of C—H in benzene
3050–3150	Stretching of C—H in imidazole

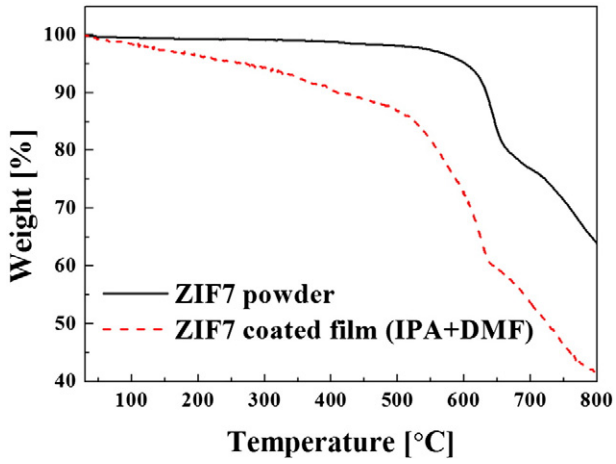

Fig. 10. Thermogravimetric analysis of pure ZIF7 powder and D–ZIF film without nylon.

The mechanism of phase transition due to cold spraying is summarized in Scheme 1. The ZIF7 structure (Phase I) shows negligible phase change at a nylon concentration of 6 wt%, as confirmed by XRD. For a lower nylon concentration, i.e., 1 wt%, the ZIF7 particles hit the substrate with partial pressure because a small amount of nylon in the solution reduces the collision impact of the particles on the substrate, forming ZIF7 Phase II, where PXRD data indicate that the majority of the six- and four-membered rings of ZIF7 are mechanically strained or stretched, but likely only some of the framework bonds break. When only IPA solvent is used, the solvent evaporates under the high temperature and pressure of the supersonic airflow, and ZIF7 particles collide with the substrate at very high speed and energy, forming Phase III by the delamination of the 3D structure to the 2D ZIF7 structure. The transformation from 3D to 2D frameworks occurs by the breakage of coordination bonds in the six-membered ZIF7 ring and the formation of four-membered rings, as explained by Peng et al. [23]. Our results demonstrate that nylon acts as an efficient intermolecular binder that lowers the impact pressure of sprayed ZIF7, thereby improving the mechanical stability of the porous framework and avoiding unwanted phase changes.

4. Conclusion

The microstructure of ZIF7 powder underwent a phase transformation from polycrystalline and porous to crystalline and dense by the pulverization of particles into a 2D phase because of the high-speed impact of the powder by supersonic cold spraying. By tuning the crystal structure of ZIF7 via supersonic spraying, customized films can be fabricated to meet the needs of various applications. This is the first successful attempt to deposit ZIF7 films by a scalable supersonic spraying method, and the structural response of ZIF7 to high-pressure impact is evident. The inclusion of 6 wt% of nylon in the precursor solvent caused the deposition of ZIF7 films with the original polycrystalline structure, similar to that of the pure powder. The absence of nylon caused a phase transformation in the sprayed film.

Acknowledgement

This research was supported by Global Frontier Program through the Global Frontier Hybrid Interface Materials (GFHIM) of the National Research Foundation of Korea (NRF) funded by the Ministry of Science, ICT & Future Planning (2013M3A6B1078879) and by the Commercializations Promotion Agency for R&D Outcomes (COMPA) funded by the Ministry of Science, ICT and Future Planning (MISP). S.S. Yoon expresses his appreciation to the Vice Deanship of Scientific Research chairs at King Saud University.

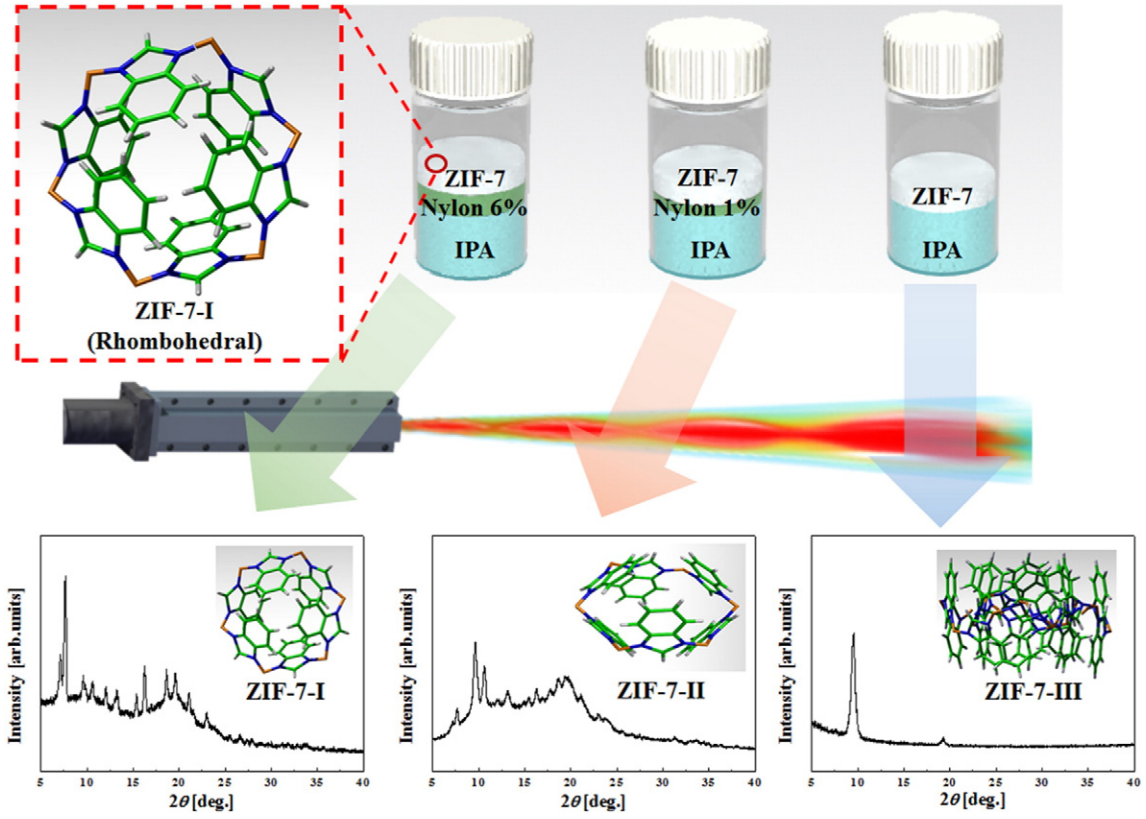

Scheme 1. The change in the crystalline structure of the supersonically sprayed ZIF7 films with varying nylon concentration.

References

[1] V.M. Aceituno Melgar, H.T. Kwon, J. Kim, Direct spraying approach for synthesis of ZIF-7 membranes by electrospray deposition, J. Membr. Sci. 459 (2014) 190–196.
[2] K. Cendrowski, P. Skumial, P. Spera, E. Mijowska, Thermally induced formation of zinc oxide nanostructures with tailoring morphology during metal organic framework (MOF-5) carbonization process, Mater. Des. 110 (2016) 740–748.
[3] T. Li, Y. Pan, K.-V. Peinemann, Z. Lai, Carbon dioxide selective mixed matrix composite membrane containing ZIF-7 nano-fillers, J. Membr. Sci. 425–426 (2013) 235–242.
[4] X. Wu, M. Niknam Shahrak, B. Yuan, S. Deng, Synthesis and characterization of zeolitic imidazolate framework ZIF-7 for CO_2 and CH_4 separation, Microporous Mesoporous Mater. 190 (2014) 189–196.
[5] W. Cai, T. Lee, M. Lee, W. Cho, D.-Y. Han, N. Choi, A.C.K. Yip, J. Choi, Thermal structural transitions and carbon dioxide adsorption properties of zeolitic imidazolate framework-7 (ZIF-7), J. Am. Chem. Soc. 136 (22) (2014) 7961–7971.
[6] X. Huang, J. Zhang, X. Chen, $[Zn(bim)_2]\cdot(H_2O)1.67$: a metal-organic open-framework with sodalite topology, Chin. Sci. Bull. 48 (15) (2003) 1531–1534.
[7] Y. Li, F. Liang, H. Bux, W. Yang, J. Caro, Zeolitic imidazolate framework ZIF-7 based molecular sieve membrane for hydrogen separation, J. Membr. Sci. 354 (1) (2010) 48–54.
[8] J. Yang, C. Zeng, F. Wei, J. Jiang, K. Chen, S. Lu, Cobalt–carbon derived from zeolitic imidazolate framework on Ni foam as high-performance supercapacitor electrode material, Mater. Des. 83 (2015) 552–556.
[9] P. Zhao, G.I. Lampronti, G.O. Lloyd, E. Suard, S.A. Redfern, Direct visualisation of carbon dioxide adsorption in gate-opening zeolitic imidazolate framework ZIF-7, J. Mater. Chem. A 2 (3) (2014) 620–623.
[10] J. Xie, N. Yan, F. Liu, Z. Qu, S. Yang, P. Liu, CO_2 adsorption performance of ZIF-7 and its endurance in flue gas components, Front. Environ. Sci. Eng. 8 (2) (2014) 162–168.
[11] C. Gücüyener, J. van den Bergh, J. Gascon, F. Kapteijn, Ethane/ethene separation turned on its head: selective ethane adsorption on the metal–organic framework ZIF-7 through a gate-opening mechanism, J. Am. Chem. Soc. 132 (50) (2010) 17704–17706.
[12] J.C. Tan, T.D. Bennett, A.K. Cheetham, Chemical structure, network topology, and porosity effects on the mechanical properties of zeolitic imidazolate frameworks, Proc. Natl. Acad. Sci. 107 (22) (2010) 9938–9943.
[13] J.C. Tan, A.K. Cheetham, Mechanical properties of hybrid inorganic–organic framework materials: establishing fundamental structure–property relationships, Chem. Soc. Rev. 40 (2) (2011) 1059–1080.
[14] S. Aguado, G. Bergeret, M.P. Titus, V. Moizan, C. Nieto-Draghi, N. Bats, D. Farrusseng, Guest-induced gate-opening of a zeolite imidazolate framework, New J. Chem. 35 (3) (2011) 546–550.
[15] P. Zhao, G.I. Lampronti, G.O. Lloyd, M.T. Wharmby, S. Facq, A.K. Cheetham, S.A. Redfern, Phase transitions in zeolitic imidazolate framework 7: the importance of framework flexibility and guest-induced instability, Chem. Mater. 26 (5) (2014) 1767–1769.
[16] M.T. Wharmby, S. Henke, T.D. Bennett, S.R. Bajpe, I. Schwedler, S.P. Thompson, F. Gozzo, P. Simoncic, C. Mellot-Draznieks, H. Tao, Extreme flexibility in a zeolitic imidazolate framework: porous to dense phase transition in desolvated ZIF-4, Angew. Chem. 127 (22) (2015) 6547–6551.
[17] M.R. Ryder, B. Civalleri, T.D. Bennett, S. Henke, S. Rudić, G. Cinque, F. Fernandez-Alonso, J.-C. Tan, Identifying the role of terahertz vibrations in metal-organic frameworks: from gate-opening phenomenon to shear-driven structural destabilization, Phys. Rev. Lett. 113 (21) (2014) 215502.
[18] Z.-X. Low, J. Yao, Q. Liu, M. He, Z. Wang, A.K. Suresh, J. Bellare, H. Wang, Crystal transformation in zeolitic-imidazolate framework, Cryst. Growth Des. 14 (12) (2014) 6589–6598.
[19] B. Zornoza, C. Tellez, J. Coronas, J. Gascon, F. Kapteijn, Metal organic framework based mixed matrix membranes: an increasingly important field of research with a large application potential, Microporous Mesoporous Mater. 166 (2013) 67–78.
[20] A. Bétard, R.A. Fischer, Metal–organic framework thin films: from fundamentals to applications, Chem. Rev. 112 (2) (2012) 1055–1083.
[21] M.D. Allendorf, V. Stavila, Crystal engineering, structure–function relationships, and the future of metal–organic frameworks, CrystEngComm 17 (2) (2015) 229–246.
[22] J. Yao, H. Wang, Zeolitic imidazolate framework composite membranes and thin films: synthesis and applications, Chem. Soc. Rev. 43 (13) (2014) 4470–4493.
[23] Y. Peng, Y. Li, Y. Ban, H. Jin, W. Jiao, X. Liu, W. Yang, Metal-organic framework nanosheets as building blocks for molecular sieving membranes, Science 346 (6215) (2014) 1356–1359.
[24] J.-G. Lee, D.-Y. Kim, B. Kang, D. Kim, S.S. Al-Deyab, S.C. James, S.S. Yoon, Thin film metallization by supersonic spraying of copper and nickel nanoparticles on a silicon substrate, Comput. Mater. Sci. 108 (2015) 114–120.
[25] D.Y. Kim, J.G. Lee, B.N. Joshi, S.S. Latthe, S.S. Al-Deyab, S.S. Yoon, Self-cleaning superhydrophobic films by supersonic-spraying polytetrafluoroethylene–titania nanoparticles, J. Mater. Chem. A. (2015).
[26] F. Meng, D. Hu, Y. Gao, S. Yue, J. Song, Cold-spray bonding mechanisms and deposition efficiency prediction for particle/substrate with distinct deformability, Mater. Des. 109 (2016) 503–510.
[27] W. Li, K. Yang, D. Zhang, X. Zhou, X. Guo, Interface behavior of particles upon impacting during cold spraying of Cu/Ni/Al mixture, Mater. Des. 95 (2016) 237–246.
[28] D.-Y. Kim, J.-J. Park, J.-G. Lee, D. Kim, S.J. Tark, S. Ahn, J.H. Yun, J. Gwak, K.H. Yoon, S. Chandra, S.S. Yoon, Cold spray deposition of copper electrodes on silicon and glass substrates, J. Therm. Spray Technol. 22 (7) (2013) 1092–1102.
[29] D.Y. Kim, S. Sinha-Ray, J.J. Park, J.G. Lee, Y.H. Cha, S.H. Bae, J.H. Ahn, Y.C. Jung, S.M. Kim, A.L. Yarin, S.S. Yoon, Self-healing reduced graphene oxide films by supersonic kinetic spraying, Adv. Funct. Mater. 24 (2014) 4986–4995.
[30] F. Li, X.X. Bao, X.F. Yu, Preparation and gas permeability of ZIF-7 membranes prepared via two-step crystallization technique, Korean Chem. Eng. Res. 52 (3) (2014) 340–346.
[31] Y.S. Li, H. Bux, A. Feldhoff, G.L. Li, W.S. Yang, J. Caro, Controllable synthesis of metal-organic frameworks: from MOF nanorods to oriented MOF membranes, Adv. Mater. 22 (30) (2010) 3322–3326.
[32] Q.-F. Yang, X.-B. Cui, J.-H. Yu, J. Lu, X.-Y. Yu, X. Zhang, J.-Q. Xu, Q. Hou, T.-G. Wang, A series of metal–organic complexes constructed from in situ generated organic amines, CrystEngComm 10 (11) (2008) 1534–1541.
[33] T.D. Bennett, D.A. Keen, J.-C. Tan, E.R. Barney, A.L. Goodwin, A.K. Cheetham, Thermal amorphization of zeolitic imidazolate frameworks, Angew. Chem. Int. Ed. 50 (13) (2011) 3067–3071.
[34] T.D. Bennett, S. Cao, J.C. Tan, D.A. Keen, E.G. Bithell, P.J. Beldon, T. Friscic, A.K. Cheetham, Facile mechanosynthesis of amorphous zeolitic imidazolate frameworks, J. Am. Chem. Soc. 133 (37) (2011) 14546–14549.
[35] W.Y. Li, C. Zhang, X.P. Guo, G. Zhang, H.L. Liao, C.J. Li, C. Coddet, Effect of standoff distance on coating deposition characteristics in cold spraying, Mater. Des. 29 (2) (2008) 297–304.
[36] J.-C. Tan, B. Civalleri, C.-C. Lin, L. Valenzano, R. Galvelis, P.-F. Chen, T.D. Bennett, C. Mellot-Draznieks, C.M. Zicovich-Wilson, A.K. Cheetham, Exceptionally low shear modulus in a prototypical imidazole-based metal-organic framework, Phys. Rev. Lett. 108 (9) (2012) 095502.
[37] J.-C. Tan, B. Civalleri, A. Erba, E. Albanese, Quantum mechanical predictions to elucidate the anisotropic elastic properties of zeolitic imidazolate frameworks: ZIF-4 vs. ZIF-zni, CrystEngComm 17 (2) (2015) 375–382.